ACS Combinatorial Science

Letter

pubs.acs.org/acscombsci

One-Pot Synthesis of Au@SiO_2 Catalysts: A Click Chemistry Approach

Vera A. Solovyeva,[†] Khanh B. Vu,[†] Zulkifli Merican,[†] Rachid Sougrat,[‡] and Valentin O. Rodionov*[,†]

[†]Division of Physical Sciences and Engineering and KAUST Catalysis Center and [‡]KAUST Advanced Nanofabrication Imaging and Characterization Core Laboratory, King Abdullah University of Science and Technology (KAUST), Thuwal, 23955-6900, Kingdom of Saudi Arabia

Supporting Information

ABSTRACT: Using the copper-catalyzed azide−alkyne cycloaddition "click" reaction, a library of triazole amphiphiles with a variety of functional polar "heads" and hydrophobic or superhydrophobic "tails" was synthesized. The amphiphiles were evaluated for their ability to stabilize small Au nanoparticles, and, at the same time, serve as templates for nanocasting porous SiO_2. One of the Au@SiO_2 materials thus prepared was found to be a highly active catalyst for the Au nanoparticle-catalyzed regioselective hydroamination of alkynes.

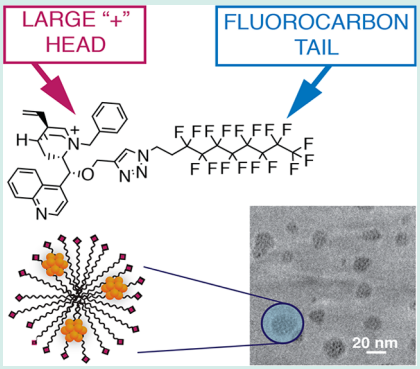

KEYWORDS: *gold nanoparticles, click chemistry, fluorous surfactant, hydroamination*

Catalysis with gold nanoparticles (AuNPs) is a topic of considerable current interest.[1] That particles be small is a prerequisite for high catalytic activity in many of the gold-catalyzed chemistries.[2] Small AuNPs have been stabilized using a variety of surface ligands,[3,4] macromolecules,[5−7] and solid supports,[8,9] such as SiO_2, Al_2O_3, and mesoporous carbon. The nature of the stabilizing ligands and supports can dramatically influence both the stability and the catalytic competency of AuNPs. Fine control over the structures of both the support and the nanoparticles is highly desirable for the development of practical catalysts.

Postsynthesis incorporation methods, such as wet impregnation/calcining,[10] immobilization of premade nanoparticles,[11] and chemical vapor deposition[12] allow full control over the structure of solid support. However, the chosen support necessarily determines the size of the nanoparticles, their spatial distribution, and surface properties. Furthermore, nanoparticles often localize close to the surface of the support, and may block the channels/pores, limiting the catalyst's accessibility.[13]

In situ incorporation methods, in which the solid support is synthesized in the presence of premade nanoparticles or the metal salt precursor, are experimentally simple and can yield materials with a uniform distribution of confined nanoparticles. This one-pot approach has been used to prepare SiO_2-supported Pd, Pt and Au nanoparticle catalysts, using polymers,[14] such as Pluronics F127[9] and P123,[15,16] chitosan,[15] or cross-linked polystyrene-*co*-polystyrenesulfonate,[17] as both nanoparticle stabilizing agents and structure-directing agents for the SiO_2 solid support. Here, we present a combinatorial approach that provides easy access to a range of SiO_2-confined AuNP materials (Au@SiO_2) based on small-molecule amphiphile templates. Using the copper-catalyzed azide−alkyne cycloaddition (CuAAC) "click" reaction,[18] we synthesized a library of triazole amphiphiles with a variety of functional polar "heads" and hydrophobic or superhydrophobic "tails". The amphiphiles were evaluated for their ability to stabilize small AuNPs,[19] and, at the same time, to serve as templates for nanocasting porous SiO_2.[20] One of the Au@SiO_2 materials thus prepared was found to be highly active catalyst for the AuNP-catalyzed regioselective hydroamination of alkynes.[6,21]

We synthesized alkyne-bearing, polar surfactant "heads" starting from cinchonidine (compounds **1a−b**) and cinchonine (compounds **2a−3b**), two readily available alkaloids. These alkaloids were chosen because we hypothesized that their quinoline and tertiary amine moieties could catalyze the hydrolysis of SiO_2 precursors and/or bind to AuNP surfaces. Two simpler alkyne "heads" were synthesized based on oligo(ethylene glycol) (compound **4**)[22] and trimethylammonium (compound **5**). Two types of hydrophobic azide "tails" were used, $C_{10}H_{21}N_3$ linear hydrocarbon and perfluorinated $C_8F_{17}CH_2CH_2N_3$. The resulting library is presented in Chart 1. The amphiphiles thus prepared were evaluated for their ability to stabilize AuNPs, and, following that, used for one-pot emulsion syntheses of Au@SiO_2 materials. We found that the morphologies of the AuNPs and the SiO_2 support were strongly influenced by the structure of the amphiphiles.

Neither of the hydrocarbon-tail cinchona surfactants **1b** or **2b** were effective stabilizers for gold nanoparticles, as extensive

Received: June 18, 2014
Revised: September 8, 2014
Published: September 17, 2014

Chart 1. Library of fluorous 1,2,3-triazole surfactants

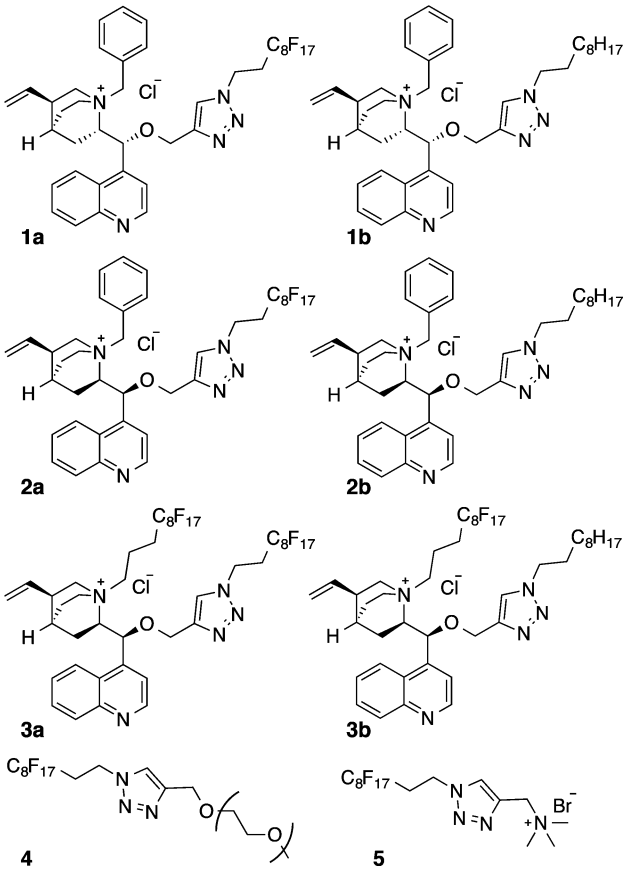

aggregation and precipitation was observed (Figure S1 D-E, Supporting Information (SI)). The neutral oligo(ethylene glycol)-based surfactant **4** was neither able to stabilize the gold nanoparticles, nor to serve as a structure-directing agent for SiO_2. The average diameter of the gold nanoparticles obtained in the presence of **4** was 12.3 nm, and there was no obvious interaction between the gold and silica (Figure S10, SI). We found that amphiphile **5** could serve as a template for structured SiO_2, although the diameters of the gold nanoparticles were far from uniform and hopelessly too big for any catalytic application (11.2 nm, Figure S11, SI).

The surfactant **3a** bearing two fluorous "tails" was capable of stabilizing somewhat smaller AuNPs, with an average diameter of 4.5 nm (Figure S9, SI). However, the structure of SiO_2 directed by **3a** was highly irregular, and low solubility of this amphiphile precluded its use in larger scale syntheses of Au@SiO_2. Likewise, the hybrid fluorous-hydrocarbon amphiphile **3b** stabilized relatively large AuNPs, as indicated by the obvious plasmonic band at ∼500 nm in the UV−vis spectrum (Figure S13, SI).

To our delight, the single-tail fluorous amphiphile **1a** and its pseudoenantiomer **2a** could stabilize small, sub-2 nm AuNPs, as indicated by the color of the colloidal solutions and the absence of plasmonic bands in the range of 500−550 nm in their UV−vis spectra[7] (Figure S1, S2 and S12, SI). The AuNP solutions stabilized by **1a** and **2a** were found to be stable for at least 10 months (Figure S3, SI).

The stereochemistry of the surfactant "head" in **1a** and **2a** did not significantly affect the ability of the amphiphiles to stabilize AuNPs. However, when the pseudoenantiomeric amphiphiles were used as structure-directing agents for the synthesis of SiO_2, markedly different morphologies of silica resulted (Figure S15, SI). Amphiphile **1a** templated highly porous, spherical, uniformly sized SiO_2 nanoparticles, with a tendency to form hollow shell structures.[23] Rod-shaped SiO_2 particles templated by **2a** were significantly smaller and more disordered. Using mixtures of **1a** and **2a** provided access to a range of spherical to rod-shaped SiO_2 morphologies. We attribute these changes in morphology to differences in the long-range order that exists in micellar assemblies of **1a**, **2a**, and their mixtures. We chose to use amphiphile **1a** for the remainder of the study due to the high porosity (Figure S7 and Table S1, SI) and regular structure of SiO_2 templated by it.

The UV−vis spectra of the **1a**-stabilized AuNPs and of the corresponding Au@SiO_2 material prepared in situ were found to be very similar to each other (Figure S2, SI), and did not show a prominent plasmonic peak. This indicates that the AuNPs growth was not significant in the presence of SiO_2 or $Si(OEt)_4$ precursor, and is supported by the size distributions of the **1a**-stabilized AuNP (Figure S3, SI) and the as-made Au@SiO_2 (Figure S4, SI). The zeta potential of the **1a**-stabilized AuNPs (Figure S6, SI) was +33.9 (±0.5) mV at pH 9.3, suggesting that the interaction between amphiphile-embedded AuNPs and SiO_2 and its precursor (negative zeta potential at high pH) came from the direct co-condensation of anionic inorganic species with the cationic surfactant.[24] After the reaction, the zeta potential of the Au@SiO_2 material was −19.6 (±1.0) mV at pH 8.7, indicating that the surfactant-stabilized AuNPs were covered by silica.

This Au@SiO_2 material retained a significant amount of amphiphile **1a** (Figure S8, SI). The as-made material is easily dispersible in perfluorodecalin and other fluorous solvents. In biphasic fluorous-hydrocarbon mixtures, the **1a**-Au@SiO_2 material partitions into the fluorous phase (Figure S16, SI). The removal of encapsulated surfactant by calcining the sample in static air at 500 °C for 4 h resulted in AuNPs with a bimodal particle size distribution (Figure 1 F and Figure S14, SI). This suggests that the remnant **1a** plays a role in the stabilization of AuNPs in the SiO_2 matrix. The calcined Au@SiO_2 completely lost its dispersibility in fluorous solvents.

Additional insight into the aggregation behavior of AuNPs and growth of SiO_2 in the presence of amphiphile **1a** was gained from cryo-transmission electron microscopy (cryo-TEM) images of the **1a**-stabilized AuNPs and corresponding Au@SiO_2 materials.

Images of AuNPs@**1a** with different electron doses are shown in Figure 1A and B. With an electron dose of 100 $e^-/Å^2$ (Figure 1A), we observed raspberry-like assemblies of low- and high-density objects, corresponding to aggregates of **1a** and AuNPs, respectively. It can be seen that **1a** forms stable and well-defined aggregates in water. The assemblies are ∼20 nm in diameter, and have a positive zeta potential (Figure S6, SI). These assemblies are remarkable in their ability to stop Ostwald ripening of small AuNPs (Figure S3, SI). To verify that the low-density objects are indeed amphiphile aggregates, we increased the electron dose from 100 to 400 $e^-/Å^2$. The low-density objects were damaged by the electron beam, as can be seen in Figure 1 B, while the high-density objects remained stable.

Cryo-TEM images of the corresponding Au@SiO_2 material with low and high electron doses are shown in Figure 1C and D. The images suggest that SiO_2 shells are growing around the AuNP@**1a** aggregates. This interaction between the SiO_2 shells and **1a**-stabilized AuNPs was confirmed by increasing the electron dose from 100 to 400 $e^-/Å^2$. The soft/organic parts of

dx.doi.org/10.1021/co5000932 | ACS Comb. Sci. 2014, 16, 513−517

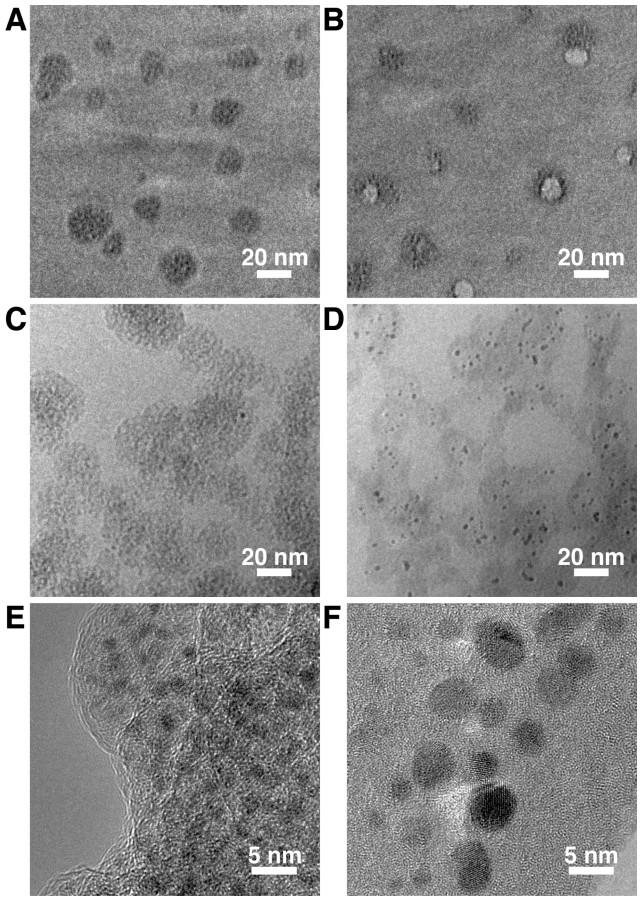

Figure 1. Cryo-TEM and TEM images of **1a**-stabilized AuNPs and Au@SiO_2 materials. (A and B) Cryo-TEM images of **1a**-stabilized AuNPs, total doses of 100 and 400 $e^-/Å^2$; (C and D) Cryo-TEM images of Au@SiO_2, total doses of 100 and 400 $e^-/Å^2$; (E and F): High resolution TEM images of as-made Au@SiO_2 and calcined Au@SiO_2.

the material (aggregates of **1a**) were damaged, while the SiO_2 shells remained intact.

We further characterized the Au@SiO_2 material prepared in the presence of **1a** using X-ray photoelectron spectroscopy (XPS) (Figure 2) and inductively coupled plasma optical emission spectroscopy (ICP-OES). The gold content determined by XPS and ICP-OES was 1.1 and 1.6 wt %, respectively. These results confirm that the material is indeed AuNPs encapsulated in SiO_2, since the apparent gold content from the surface analysis (XPS) is lower than that from the bulk analysis (ICP-OES).[25] Since Au $4f_{7/2}$ and $4f_{5/2}$ of the Au 4f spectrum of Au@SiO_2 were not well separated and broad compared with those of the Au 4f spectrum of the Au^0 film, more than one valence state of Au should be expected. We attributed the Au $4f_{7/2}$ at 83.87 eV and that at 84.60 eV to Au^0 and $Au^{\delta+}$, respectively.[26] The assignment of the partially charged $Au^{\delta+}$ (~40% of total Au present) in this case was neither Au^+ (85.6 eV) nor Au^{3+} (87.5 eV), for which the binding energies are well established.[27] A possible explanation for this observation is that the low and high binding energy represents the bulk (core) and surface (the shell interacting with the fluorinated surfactant) of the AuNPs, respectively. The same observation was made for thiolate-protected AuNPs.[4,28]

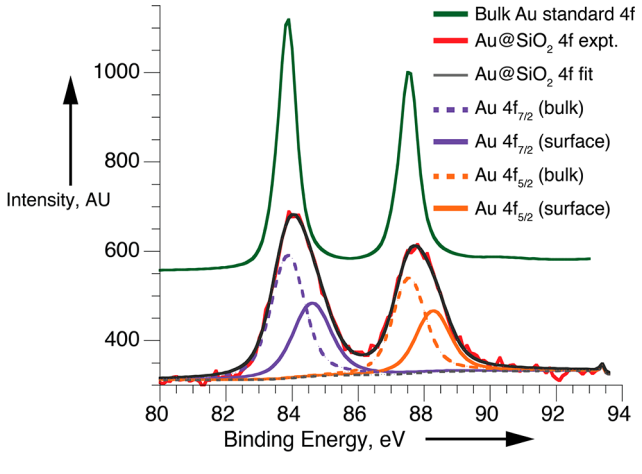

Figure 2. XPS spectra of the Au 4f level.

The Au@SiO_2 material, prepared in the presence of **1a**, exhibited excellent activity and 100% selectivity for the imine products when used in hydroamination of alkynes with anilines (Table 1). It is important to note that for each of the reactions

Table 1. Hydroamination of Alkynes with Anilines[a]

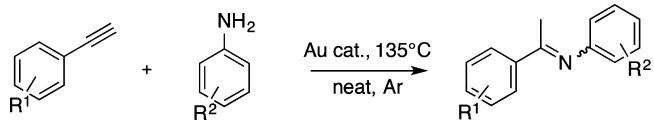

entry	R^1	R^2	time (h)	alkyne conv. (%)[b]	TON
1	H	H	16	97	1605
2	*p*-Et	H	16	100	1640
3	*p*-PhO	H	16	93	1361
4	*p*-C_5H_{11}	H	16	100	1640
5	1-ethynyl-naphthalene	H	16	98	1605
6	H	*p*-MeO	16	100	1640
7	*p*-Et	*p*-MeO	16	100	1640
8	*p*-PhO	*p*-MeO	16	100	1640
9	*p*-C_5H_{11}	*p*-MeO	16	95	1560
10	1-ethynyl-naphthalene	*p*-MeO	16	99	1619
11	H	*p*-Me	16	88	1441
12	*p*-Et	*p*-Me	16	92	1514
13	*p*-C_5H_{11}	*p*-Me	16	94	1534
14	1-ethynyl-naphthalene	*p*-Me	16	99	1626
15	2,4-di(CF_3)	H	36	60	984
16	H	2,4-di(CF_3)	36	77	1263
17	H	H	16	97[c]	1605[c]
18	*p*-Et	H	16	83[c]	1361[c]
19	*p*-PhO	H	16	77[c]	1256[c]

[a]Reaction conditions: 1 mmol of acetylene, 1.5 mmol of aniline, 7.5 mg of as-made catalyst (0.61 mmol, 0.61×10^{-3} eq Au), under Ar, 135 °C. [b]Determined by GC/MS with chlorobenzene as internal standard; [c]With calcined catalyst (3.2 mg, 0.61 mmol, 0.61×10^{-3} equiv of Au).

in the Table, the corresponding blank reactions did not lead to the formation of any imine product. The optimal reaction conditions were achieved by using a neat mixture of 1 equiv of alkyne and 1.5 equiv of aniline under Ar atmosphere at 135 °C for 16 h. These conditions led to an almost quantitative conversion of the alkyne to an imine for most of the substrates,

dx.doi.org/10.1021/co5000932 | ACS Comb. Sci. 2014, 16, 513−517

with only a trace amount of a hydrolysis byproduct (corresponding acetophenone). The presence of electron-donating substituents in both the alkyne and aniline substrates activated them for hydroamination (Table 1, entries 2−14). The reactions were markedly slowed by electron-withdrawing substituents (Table 1, entries 15−16).

We compared the catalytic efficiency of the as-made and calcined Au@SiO_2 materials (same Au loading as determined by ICP-OES). The as-made Au@SiO_2 catalyst containing amphiphile **1a** was found to be catalytically more effective for hydroamination of alkynes. The activity of the calcined catalyst was similar to the as-made material for the reaction of phenylacetylene with aniline (Table 1, entries 1 and 17). However, the calcined material exhibited markedly lower activity for substituted phenylacetylenes and anilines (Table 1, entries 2, 3, 18, and 19). As determined by nitrogen sorption (Figure S7 and Table S1, SI) the Au surface of the calcined Au@SiO_2 should be more accessible than that of the as-made Au@SiO_2, since the surfactant in the as-made material could slow the diffusion of the substrates and products. Thus, the difference in activity between the two samples is due to the difference in AuNP size. The smaller particles in the as-made catalyst are stabilized by the remnant **1a**. Since SiO_2 has a strongly negative ζ-potential, **1a**-stabilized AuNPs tend to remain inside the SiO_2 matrix. Leaching of Au into the reaction medium was explored by ICP-OES, after incubating the catalyst under typical reaction conditions at 130 °C for 16 h. No significant leaching has been observed (see SI).

In conclusion, we screened a library of triazole-based surfactants for their ability to stabilize Au nanoparticles in aqueous solution. We determined that at least one perfluorinated hydrophobic "tail" combined with a large cationic "head" in the surfactant molecule is necessary to stabilize small, catalytically competent AuNPs. Au@SiO_2 materials prepared in the presence of amphiphile **1a** exhibited high turnover numbers and selectivity in hydroamination of alkynes with anilines. Our combinatorial approach to the surfactant-templated nanoparticle@SiO_2 materials is general; we are now applying it in our laboratories to the synthesis of other catalysts and porous oxide supports.

■ ASSOCIATED CONTENT

Ⓢ Supporting Information

Complete experimental details, characterization (1D and 2D ^{1}H, ^{13}C, and ^{19}F NMR and FTIR spectra), and additional TEM images. This material is available free of charge via the Internet at http://pubs.acs.org/.

■ AUTHOR INFORMATION

Corresponding Author

*E-mail: valentin.rodionov@kaust.edu.sa. Tel: +966-12-8084592.

Author Contributions

V.A.S. and K.B.V. contributed equally.

Notes

The authors declare no competing financial interest.

■ ACKNOWLEDGMENTS

Support from KAUST baseline funding program is acknowledged with thanks.

■ REFERENCES

(1) (a) Haruta, M. When Gold is Not Noble: Catalysis By Nanoparticles. *Chem. Rec.* **2003**, *3*, 75−87. (b) Mikami, Y.; Dhakshinamoorthy, A.; Alvaro, M.; Garcia, H. Catalytic Activity of Unsupported Gold Nanoparticles. *Catal. Sci. Technol.* **2013**, *3*, 58−69. (c) Corma, A.; Leyva-Pérez, A.; Sabater, M. J. Gold-Catalyzed Carbon-Heteroatom Bond-Forming Reactions. *Chem. Rev.* **2011**, *111*, 1657−1712.

(2) (a) Turner, M.; Golovko, V. B.; Vaughan, O. P. H.; Abdulkin, P.; Berenguer-Murcia, A.; Tikhov, M. S.; Johnson, B. F. G.; Lambert, R. M. Selective Oxidation With Dioxygen By Gold Nanoparticle Catalysts Derived From 55-Atom Clusters. *Nature* **2008**, *454*, 981−983. (b) Corma, A.; Garcia, H. Supported Gold Nanoparticles as Catalysts for Organic Reactions. *Chem. Soc. Rev.* **2008**, *37*, 2096−2126.

(3) (a) Brust, M.; Walker, M.; Bethell, D.; Schiffrin, D. J.; Whyman, R. Synthesis of Thiol-Derivatised Gold Nanoparticles in a Two-Phase Liquid-Liquid System. *J. Chem. Soc., Chem. Commun.* **1994**, 801−802. (b) Zhang, L.; Sun, X.; Song, Y.; Jiang, X.; Dong, S.; Wang, E. Didodecyldimethylammonium Bromide Lipid Bilayer-Protected Gold Nanoparticles: Synthesis, Characterization, and Self-Assembly. *Langmuir* **2006**, *22*, 2838−2843.

(4) Negishi, Y.; Nobusada, K.; Tsukuda, T. Glutathione-Protected Gold Clusters Revisited: Bridging the Gap Between Gold(I)−Thiolate Complexes and Thiolate-Protected Gold Nanocrystals. *J. Am. Chem. Soc.* **2005**, *127*, 5261−5270.

(5) (a) Daiel, M.-C.; Astruc, D. Gold Nanoparticles: Assembly, Supramolecular Chemistry, Quantum-Size-Related Properties, and Applications Toward Biology, Catalysis, and Nanotechnology. *Chem. Rev.* **2003**, *104*, 293−346. (b) Dioos, B. M. L.; Vankelecom, I. F. J.; Jacobs, P. A. Aspects of Immobilisation of Catalysts on Polymeric Supports. *Adv. Synth. Catal.* **2006**, *348*, 1413−1446.

(6) Corma, A.; Concepción, P.; Domínguez, I.; Forné, V.; Sabater, M. J. Gold Supported on a Biopolymer (Chitosan) Catalyzes the Regioselective Hydroamination of Alkynes. *J. Catal.* **2007**, *251*, 39−47.

(7) Kim, Y.-G.; Oh, S.-K.; Crooks, R. M. Preparation and Characterization of 1−2 nm Dendrimer-Encapsulated Gold Nanoparticles Having Very Narrow Size Distributions. *Chem. Mater.* **2003**, *16*, 167−172.

(8) (a) Chen, J.; Zhang, R.; Han, L.; Tu, B.; Zhao, D. One-Pot Synthesis of Thermally Stable Gold@Mesoporous Silica Core-Shell Nanospheres With Catalytic Activity. *Nano Res.* **2013**, *6*, 871−879. (b) Chen, L.; Hu, J.; Richards, R. Intercalation of Aggregation-Free and Well-Dispersed Gold Nanoparticles Into the Walls of Mesoporous Silica as a Robust "Green" Catalyst for N-Alkane Oxidation. *J. Am. Chem. Soc.* **2008**, *131*, 914−915. (c) Gajan, D.; Guillois, K.; Delichère, P.; Basset, J.-M.; Candy, J.-P.; Caps, V.; Coperet, C.; Lesage, A.; Emsley, L. Gold Nanoparticles Supported on Passivated Silica: Access to an Efficient Aerobic Epoxidation Catalyst and the Intrinsic Oxidation Activity of Gold. *J. Am. Chem. Soc.* **2009**, *131*, 14667−14669. (d) Liu, Y.; Tsunoyama, H.; Akita, T.; Tsukuda, T. Preparation of ∼1 nm Gold Clusters Confined Within Mesoporous Silica and Microwave-Assisted Catalytic Application for Alcohol Oxidation. *J. Phys. Chem. C* **2009**, *113*, 13457−13461. (e) Zhu, F.-X.; Wang, W.; Li, H.-X. Water-Medium and Solvent-Free Organic Reactions Over a Bifunctional Catalyst With Au Nanoparticles Covalently Bonded to HS/SO_3H Functionalized Periodic Mesoporous Organosilica. *J. Am. Chem. Soc.* **2011**, *133*, 11632−11640.

(9) Wang, S.; Zhao, Q.; Wei, H.; Wang, J.-Q.; Cho, M.; Cho, H. S.; Terasaki, O.; Wan, Y. Aggregation-Free Gold Nanoparticles in Ordered Mesoporous Carbons: Toward Highly Active and Stable Heterogeneous Catalysts. *J. Am. Chem. Soc.* **2013**, *135*, 11849−11860.

(10) (a) Köhn, R.; Fröba, M. Nanoparticles of 3d Transition Metal Oxides in Mesoporous MCM-48 Silica Host Structures: Synthesis and Characterization. *Catal. Today* **2001**, *68*, 227−236. (b) Wang, Z.; Xie, Y.; Liu, C.-J. Synthesis and Characterization of Noble Metal (Pd, Pt, Au, Ag) Nanostructured Materials Confined in the Channels of Mesoporous SBA-15. *J. Phys. Chem. C* **2008**, *112*, 19818−19824. (c) Scott, R. W. J.; Wilson, O. M.; Crooks, R. M. Titania-Supported

Au and Pd Composites Synthesized From Dendrimer-Encapsulated Metal Nanoparticle Precursors. *Chem. Mater.* **2004**, *16*, 5682−5688.
(11) (a) Wittmann, S.; Schätz, A.; Grass, R. N.; Stark, W.; Reiser, O. A Recyclable Nanoparticle-Supported Palladium Catalyst for the Hydroxycarbonylation of Aryl Halides in Water. *Angew. Chem., Int. Ed.* **2010**, *49*, 1867−1870. (b) Malynych, S.; Luzinov, I.; Chumanov, G. Poly(Vinyl Pyridine) as a Universal Surface Modifier for Immobilization of Nanoparticles. *J. Phys. Chem. B* **2002**, *106*, 1280−1285.
(12) (a) Dossi, C.; Psaro, R.; Bartsch, A.; Fusi, A.; Sordelli, L.; Ugo, R.; Bellatreccia, M.; Zanoni, R.; Vlaic, G. Chemical Vapor Deposition of Platinum Hexafluoroacetylacetonate Inside KL Zeolite: A New Route to Nonacidic Platinum-in-Zeolite Catalysts. *J. Catal.* **1994**, *145*, 377−383. (b) Gary, J.; Sandrine, R.; Patricia, M. P.; Uschi, M. G.; Alan, D.; Syed, K.; Elin, R.; Burtron, H. D. Low Temperature Water-Gas Shift: Examining the Efficiency of Au as a Promoter for Ceria-Based Catalysts Prepared By CVD of an Au Precursor. *Appl. Catal., A* **2005**, *292*, 229−243.
(13) (a) Cai-Hua, T.; Ai-Qin, W.; Ming-Yuan, Z.; Xiao-Dong, W.; Tao, Z. Factors Influencing the Catalytic Activity of SBA-15-Supported Copper Nanoparticles in Co Oxidation. *Appl. Catal., A* **2006**, *297*, 40−47. (b) Bronstein, L. M.; Chernyshov, D. M.; Karlinsey, R.; Zwanziger, J. W.; Matveeva, V. G.; Sulman, E. M.; Demidenko, G. N.; Hentze, H.-P.; Antonietti, M. Mesoporous Alumina and Aluminosilica With Pd and Pt Nanoparticles: Structure and Catalytic Properties. *Chem. Mater.* **2003**, *15*, 2623−2631.
(14) Bronstein, L.; Krämer, E.; Berton, B.; Burger, C.; Förster, S.; Antonietti, M. Successive Use of Amphiphilic Block Copolymers as Nanoreactors and Templates: Preparation of Porous Silica With Metal Nanoparticles. *Chem. Mater.* **1999**, *11*, 1402−1405.
(15) Gaweł, B.; Lambrechts, K.; Gaweł, K.; Øye, G. One-Pot Synthesis of Gold Nanoparticle Functionalised Mesoporous Silica—The Double Role of a Tri-Block Copolymer and Chitosan. *Micropor. Mesopor. Mater.* **2012**, *164*, 32−37.
(16) Li, L.; Jin, C.; Wang, X.; Ji, W.; Pan, Y.; van der Knaap, T.; van der Stoel, R.; Au, C. T. Cyclohexane Oxidation Over Size-Uniform Au Nanoparticles (SBA-15 Hosted) in a Continuously Stirred Tank Reactor Under Mild Conditions. *Catal. Lett.* **2009**, *129*, 303−311.
(17) Whilton, N. T.; Berton, B.; Bronstein, L.; Hentze, H.-P.; Antonietti, M. Organized Functionalization of Mesoporous Silica Supports Using Prefabricated Metal-Polymer Modules. *Adv. Mater.* **1999**, *11*, 1014−1018.
(18) (a) Tornøe, C. W.; Christensen, C.; Meldal, M. Peptidotriazoles on Solid Phase: [1,2,3]-Triazoles By Regiospecific Copper(I)-Catalyzed 1,3-Dipolar Cycloadditions of Terminal Alkynes to Azides. *J. Org. Chem.* **2002**, *67*, 3057−3062. (b) Rostovtsev, V. V.; Green, L. G.; Fokin, V. V.; Sharpless, K. B. A Stepwise Huisgen Cycloaddition Process: Copper(I)-Catalyzed Regioselective Ligation of Azides and Terminal Alkynes. *Angew. Chem., Int. Ed.* **2002**, *41*, 2596−2599.
(19) (a) Aprile, C.; Abad, A.; Garcia, H.; Corma, A. Synthesis and Catalytic Activity of Periodic Mesoporous Materials Incorporating Gold Nanoparticles. *J. Mater. Chem.* **2005**, *15*, 4408−4413. (b) Premkumar, T.; Kim, D.; Lee, K.; Geckeler, K. E. A Facile and Efficient "One-Step" Synthesis of Au^0 With Tunable Size. *Gold Bull.* **2007**, *40*, 321−327. (c) Gao, J.; Bender, C. M.; Murphy, C. J. Dependence of the Gold Nanorod Aspect Ratio on the Nature of the Directing Surfactant in Aqueous Solution. *Langmuir* **2003**, *19*, 9065−9070.
(20) Polarz, S.; Antonietti, M. Porous Materials Via Nanocasting Procedures: Innovative Materials and Learning About Soft-Matter Organization. *Chem. Commun.* **2002**, 2593−2604.
(21) (a) Widenhoefer, R. A.; Han, X. Gold-Catalyzed Hydroamination of C−C Multiple Bonds. *Eur. J. Org. Chem.* **2006**, *2006*, 4555−4563. (b) Alonso, F.; Beletskaya, I. P.; Yus, M. Transition-Metal-Catalyzed Addition of Heteroatom−Hydrogen Bonds to Alkynes. *Chem. Rev.* **2004**, *104*, 3079−3160. (c) Zhao, J.; Zheng, Z.; Bottle, S.; Chou, A.; Sarina, S.; Zhu, H. Highly Efficient and Selective Photocatalytic Hydroamination of Alkynes By Supported Gold Nanoparticles Using Visible Light At Ambient Temperature. *Chem. Commun.* **2013**, *49*, 2676−2678. (d) Seral-Ascaso, A.; Luquin, A.; Lázaro, M. J.; de la Fuente, G. F.; Laguna, M.; Muñoz, E. Synthesis and Application of Gold−Carbon Hybrids as Catalysts for the Hydroamination of Alkynes. *Appl. Catal., A* **2013**, *456*, 88−95.
(22) Francis, D. V.; Miles, D. H.; Mohammed, A. I.; Read, R. W.; Wang, X. Towards Functional Fluorous Surfactants. Synthesis of Hydrophilic Fluorous 1,2,3-Triazolylmethyl Ethers and Di(1,2,3-Triazolylmethyl) Ethers. *J. Fluorine Chem.* **2011**, *132*, 898−906.
(23) Tan, B.; Lehmler, H. J.; Vyas, S. M.; Knutson, B. L.; Rankin, S. E. Fluorinated-Surfactant-templated Synthesis of Hollow Silica Particles With a Single Layer of Mesopores in Their Shells. *Adv. Mater.* **2005**, *17*, 2368−2371.
(24) Huo, Q.; Margolese, D. I.; Ciesla, U.; Feng, P.; Gier, T. E.; Sieger, P.; Leon, R.; Petroff, P. M.; Schuth, F.; Stucky, G. D. Generalized Synthesis of Periodic Surfactant/Inorganic Composite Materials. *Nature* **1994**, *368*, 317−321.
(25) (a) Serpell, C. J.; Cookson, J.; Ozkaya, D.; Beer, P. D. Core@Shell Bimetallic Nanoparticle Synthesis Via Anion Coordination. *Nat. Chem.* **2011**, *3*, 478−483. (b) Zesheng, L.; Chunyong, H.; Mei, C.; Shuai, K.; Pei, K. S. A Strategy for Easy Synthesis of Carbon Supported Co@Pt Core−Shell Configuration as Highly Active Catalyst for Oxygen Reduction Reaction. *Int. J. Hydrogen Energy* **2012**, *37*, 14152−14160.
(26) Moulder, J. F.; Stickle, W. F.; Sobol, P. E.; Bomben, K. D. *Handbook of X-Ray Photoelectron Spectroscopy: A Reference Book of Standard Spectra for Identification and Interpretation of XPS Data*; Perkin-Elmer Corporation: Eden Prairie, MN, 1992; p 261.
(27) Salama, T. M.; Shido, T.; Minagawa, H.; Ichikawa, M. Characterization of Gold(I) in NaY Zeolite and Acidity Generation. *J. Catal.* **1995**, *152*, 322−330.
(28) (a) Ohta, T.; Shibuta, M.; Tsunoyama, H.; Negishi, Y.; Eguchi, T.; Nakajima, A. Size and Structure Dependence of Electronic States in Thiolate-Protected Gold Nanoclusters of $Au_{25}(SR)_{18}$, $Au_{38}(SR)_{24}$, and $Au_{144}(SR)_{60}$. *J. Phys. Chem. C* **2013**, *117*, 3674−3679. (b) Tanaka, A.; Takeda, Y.; Imamura, M.; Sato, S. Dynamic Final-State Effect on the Au 4f Core-Level Photoemission of Dodecanethiolate-Passivated Au Nanoparticles on Graphite Substrates. *Phys. Rev. B* **2003**, *68*, No. 195415.